Ecography

ECOG-00697
Tovar, C., Breman, E., Brncic, T., Harris, D. J., Bailey, R. and Willis, K. J. 2014. Influence of 1100 years of burning on the central African rainforest. – Ecography doi: 10.1111/ecog.00697

Supplementary material

Appendix 1.

Vegetation description of each core

We recorded the main species present at each site where cores were collected and assigned a preliminary forest type based on this data. Swamp forest was easily identified. To further corroborate our designation of *Gilbertiodendron*, Mixed and Marantaceae forest we used available classifications of satellite images (Devos et al. 2008) to determine the forest surrounding the core sites using a buffer of 200 m radius. This analysis (Fig. A1) gave us percentage values of open vs closed canopy which we used to assign the forest type as follows: Swamp forest (sites 1, 8 and 9) was characterized by more than 50% of semi-open and open canopy cover and included typically swampy species. Mixed forest (sites 5, 6, 10, 15 and 16) was characterised by closed canopy cover (closed canopy and closed canopy *Gilbertiodendron*) of more than 50% but the class "closed canopy *Gilbertiodendron*" covers less than 50% of the area within the 200 m radius. In cases when at least 50% of the land cover was represented by the class "closed canopy *Gilbertiodendron*", the core site was assigned as monodominant *Gilbertiodendron* forest (sites 7 and 14). Finally, we assigned the class Marantaceae forest to core sites with more than 50% of semi open and open canopy cover, and where the presence of patches of *Megaphrynium macrostachyum* was recorded (sites 13 and 17). Site 17 also has *Haumania liebrechtsiana*, and a more open canopy than site 13. The location and details relating to each core are shown in Table 1.

Using the same classification we calculated the distance of each site of collection to the nearest different forest type (Table A1).

References

Devos, C. et al. 2008. Comparing Ape Densities and Habitats in Northern Congo: Surveys of Sympatric Gorillas and Chimpanzees in the Odzala and Ndoki Regions. - Am. J. Primatol. 70: 1–13.

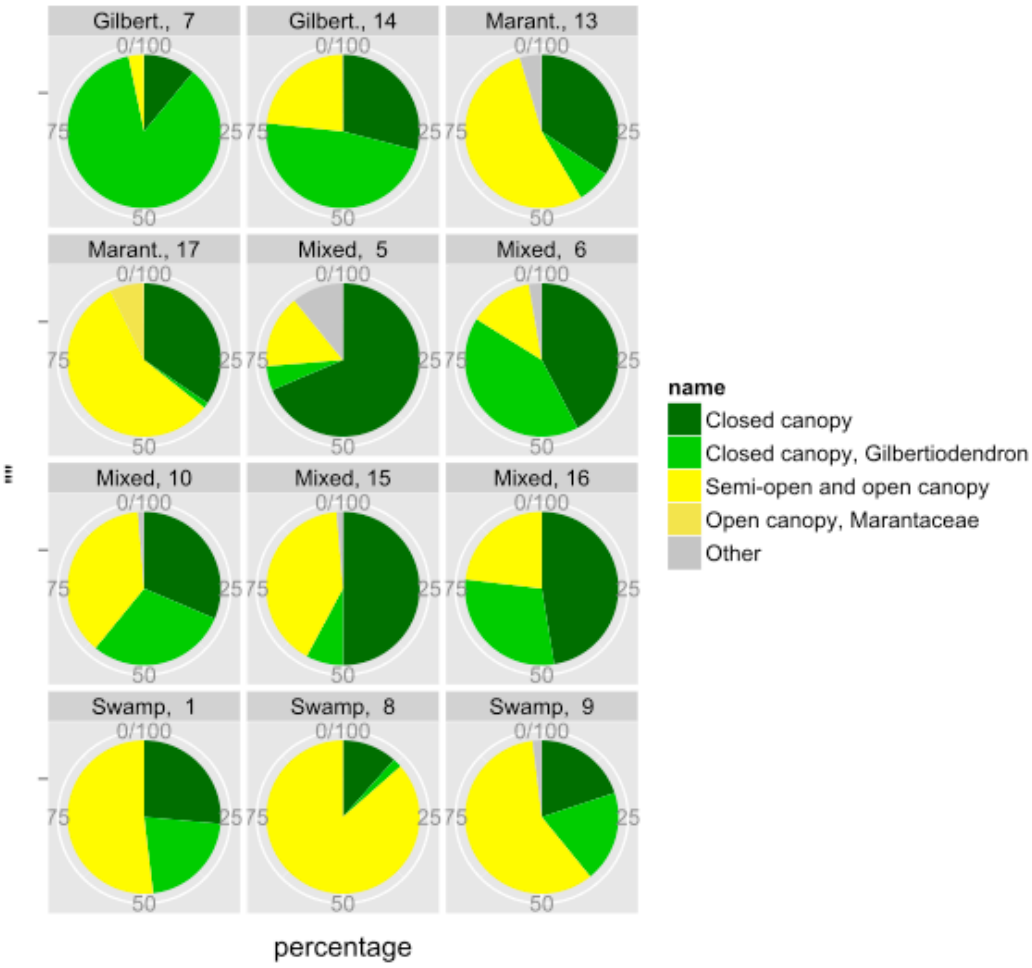

Figure A1. Forest coverage in percentage for every site.

Table A1. Distance to the nearest different forest type for each site of core collection

Id core	Current forest type	Nearest forest	Distance to the nearest forest at present (m)
Site 1	Swamp	Mixed	800
Site 8	Swamp	Mixed	1100
Site 9	Swamp	Mixed	1300
Site 13	Marantaceae	Swamp	2000
Site 17	Marantaceae	Swamp	1500
Site 7	*Gilbertiodendron*	Mixed	500
Site 14	*Gilbertiodendron*	Mixed	500
Site 5	Mixed	*Gilbertiodendron*	1800
Site 6	Mixed	*Gilbertiodendron*	500
Site 10	Mixed	Swamp	2500
Site 15	Mixed	*Gilbertiodendron*	2000
Site 16	Mixed	*Gilbertiodendron*	500

Appendix 2.

Optically stimulated luminescence dating (OSL)

Luminescence methods provide estimates of the total radiation dose absorbed (D_e, units Gy) by sedimentary grains during burial. Estimation of burial age (in units ka, thousands of years) is possible if the mean radiation dose rate (D', units Gy/ka) is known, and in this case Age = D_e/D' (Aitken 1998).

Sediment samples from the sediment cores were extracted for optical dating under laboratory conditions. The exposed face of the sediment core was excavated to a depth of 20 mm under subdued amber (580 nm) lighting (demonstrated to have negligible effects on quartz OSL signals). The samples were processed under the same lighting conditions in order to extract refined quartz grains. Each sample was washed in distilled water to remove <15μm material and sieved, retaining the 180-250 μm fraction. This material was immersed for two days in 1 M HCl to remove carbonate, washed in distilled water, immersed for two days in H_2O_2 to remove organic matter, and washed again in water. Heavy minerals (density >2.72 g/cm^3) were removed from the treated sample fraction by heavy liquid (sodium polytungstate) separation. The <2.72 g/cm^3 fractions were then etched with 48% HF for 60 minutes, followed by HCl and water rinses to remove precipitates. The HF treatment removes potassium feldspar and etches the outer (alpha-irradiated) surface of the quartz grains. The remaining quartz grains were re-sieved to the original grains size range. Sub-samples of each prepared quartz sample were mounted for single grain measurement.

Optically stimulated luminescence measurements were made using an automated Risø TL/OSL DA-15 reader (Botter-Jensen et al. 2000), with single-grain attachment. Optical stimulation of individual quartz grains was achieved using a 10 mW Nd:YVO_4 diode pumped laser, providing approximately 50 W cm^{-2} in a focused 30 μm spot at 532 nm to each grain. IR stimulation of the sample disc was provided by diodes at 880 nm (approx. 400 mW cm^{-2}). Samples were irradiated using a calibrated ^{90}Sr/^{90}Y beta source. The ultra-violet (~370 nm) component of the emitted luminescence was measured using a photomultiplier (type 9235QA) filtered with two Corning U-340 glass filters. Equivalent doses were determined using the Single-Aliquot Regenerative-dose (SAR) procedure (Wintle and Murray 2006). Samples were preheated for 10 s at 260°C prior to measurement of natural and regenerative dose (L_x) points, and for 10 s at 220°C prior to the sensitivity correction (T_x) measurements. All OSL measurements were made at 130°C.

Grains were selected for inclusion in D_e analysis which passed the following criteria: 'recycling ratio' and 'IR depletion ratio' within 10% and/or 2σ of unity, 'zero-dose ratio' within 10% and/or 2σ of zero, dose response data successfully described by the fitted 'exponential-plus-linear' function. Fitting success was defined as the fit passing within 1σ of each L_x/T_x point. This is a rather conservative criterion but judged appropriate given the ratio of data points to fitted parameters (six regeneration points and four free parameters). The statistical uncertainties on each L_x/T_x measurement were based on counting statistics and were propagated through to an uncertainty on D_e (σD_e) using a Monte Carlo procedure (each growth curve dataset being sampled 1000 times); a further systematic uncertainty of 3% was added in quadrature to each σD_e value to account for calibration errors and machine reproducibility. Grains with relatively low sensitivity were included in the analysis but naturally contributed little to the estimate of D_e due to the weighting of individual estimates. Depending on raw sample size (sampled volume and quartz yield) and the proportion of luminescent grains, between approximately 300 and 700 grains were measured for each sample. Of these, the number of 'successful grains' (n) used for D_e estimation is given in Table A2.

For each sample, the degree of skewness in D_e values (weighted by uncertainty in each D_e estimate) was significant at 95% (Bailey and Arnold 2006). An example is shown in Figure A2 for sample Con09-10-86 (skewness=2.5; threshold for 95% significance is 0.68). Given the depositional environment and the significant degree of skewness observed, these samples are interpreted as having been heterogeneously (partially) bleached prior to deposition (see Bailey and Arnold 2006 for discussion). The Minimum Age Model (MAM) of Galbraith et al.(Galbraith et al. 1999) was used to estimate D_e (implemented using the S script circulated amongst the luminescence community by Dr Rex Galbraith) apart from in cases where no numerical solution could be found or where individual low D_e estimates produced a dominant effect resulting in dates being out of stratigraphic order. For these cases (approx. 30% of the samples), the Finite Mixture Model (e.g. Jacobs et al. 2008) was used to estimate D_e, taking the first component greater than the low-lying estimate. In the present case this is a suboptimal solution to the problem of estimating D_e from scattered natural dose populations with low 'outliers' but was deemed preferable to other options, such as the outright rejection of samples.

During burial, the radiation dose-rate (D') comprises contributions from β-, γ-, and cosmic-radiation (Aitken 1998). The β and γ components of D' result from the radioactive

decay series of ^{238}U, ^{232}Th and from ^{40}K within the sediment. These parent isotopes were measured using Inductively Coupled Plasma Mass-Spectrometry (ICP-MS) and their decay products were assumed to be in constant abundance throughout the burial period. The measured radionuclide concentrations were converted directly to estimates of D' (Adamiec and Aitken 1998), assuming a water content of 17±7% (water mass as a fraction of total wet sediment mass; a value of 50% saturation was chosen for dose rate calculations, defined from porosity measurements on a subset of samples, with errors conservatively estimated as 50% of the saturation value) and correcting for size-dependent β-attenuation through the quartz grains. The cosmic dose contribution to D' was calculated according to (Prescott and Hutton 1994), assuming an overburden density of 2 g/cm^3, taking in to account sampled depth, site altitude and geomagnetic latitude.

The final age uncertainty in each case includes uncertainties on D_e values (which include errors due to photon-counting statistics, curve fitting/interpolation, source calibration, machine reproducibility), all isotope concentrations, dose-rate conversion factors; attenuation/absorption factors, water content, burial depth and overburden density. A data summary is given in Table A2.

References

Adamiec, G. and Aitken, M. 1998. Dose-rate conversion factors: update. - Anc. TL 16: 37–50.

Aitken, M. 1998. An Introduction to Optical Dating. - Oxford University Press.

Bailey, R. M. and Arnold, L. J. 2006. Statistical modelling of single grain quartz De distributions and an assessment of procedures for estimating burial dose. - Quat. Sci. Rev. 25: 2475–2502.

Botter-Jensen, L. et al. 2000. Advances in luminescence instrument systems. - Radiat. Meas. 32: 523–528.

Galbraith, R. H. et al. 1999. Optical dating of single and multiple grains of quartz from Jinmium rock shelter, northern Australia: Part I, Experimental design and statistical models. - Archaeometry 41: 339–364.

Jacobs, Z. et al. 2008. New ages for the post-Howiesons Poort, late and final Middle Stone Age at Sibudu, South Africa. - J. Archaeol. Sci. 35: 1790–1807.

Prescott, J. R. and Hutton, J. T. 1994. Cosmic ray contributions to dose rates for luminescence and ESR dating: Large depths and long-term time variations. - Radiat. Meas. 23: 497–500.

Wintle, A. G. and Murray, A. S. 2006. A review of quartz optically stimulated luminescence characteristics and their relevance in single-aliquot regeneration dating protocols. - Radiat. Meas. 41: 369–391.

Table A2. Summary data for calculation of OSL ages. D_e is the 'equivalent dose' (the estimate of the total absorbed radiation dose), and n is the number of grains accepted according to the selection criteria described in the main text. All other values are as described in the main text.

Sample ID	**CON09-1-2**	**CON09-1-12**	**CON09-1-26**	**CON09-1-38**	**CON09-1-60**	**CON09-1-100**
D_e (Gy)	0.04 ± 0.004	0.37 ± 0.05	0.81 ± 0.14	1.48 ± 0.22	1.73 ± 0.19	2.16 ± 0.1
n	135	54	65	48	111	129
Depth (m)	0.02 ± 0.01	0.12 ± 0.05	0.26 ± 0.05	0.38 ± 0.04	0.6 ± 0.05	1 ± 0.1
Min. grain size (mm)	150-210	150-210	150-210	150-210	150-210	150-210
U (ppm)	0.87 ± 0.09	0.87 ± 0.09	1.13 ± 0.11	1.15 ± 0.11	1.18 ± 0.12	1.18 ± 0.12
Th (ppm)	8.91 ± 0.89	8.68 ± 0.87	10.38 ± 1.04	10.24 ± 1.02	9.98 ± 1	10.22 ± 1.02
K (%)	0.033 ± 0.002	0.025 ± 0.001	0.025 ± 0.001	0.025 ± 0.001	0.025 ± 0.001	0.025 ± 0.001
Moisture (%)	17 ± 7	17 ± 7	17 ± 7	17 ± 7	17 ± 7	17 ± 7
Cosmic D' (Gy/ka)	0.2 ± 0.1	0.2 ± 0.08	0.2 ± 0.04	0.19 ± 0.02	0.19 ± 0.02	0.18 ± 0.02
Total D' (Gy/ka)	0.89 ± 0.13	0.87 ± 0.11	1.01 ± 0.1	1.01 ± 0.1	0.99 ± 0.09	0.99 ± 0.1
Age (years)	45 ± 8	424 ± 80	800 ± 160	1471 ± 260	1746 ± 253	2173 ± 233
Sample ID	**CON09-5-2**	**CON09-5-22**	**CON09-6-2**	**CON09-6-22**	**CON09-6-42**	**CON09-6-76**
D_e (Gy)	0.05 ± 0.01	0.96 ± 0.09	0.12 ± 0.13	0.41 ± 0.1	2.22 ± 0.09	4.03 ± 0.21
n	32,000	62,000	37,000	41,000	28	9,000
Depth (m)	0.02 ± 0.01	0.22 ± 0.05	0.02 ± 0.01	0.22 ± 0.05	0.42 ± 0.05	0.76 ± 0.05
Min. grain size (mm)	150-210	150-210	150-210	150-210	150-210	150-210
U (ppm)	1.13 ± 0.11	0.78 ± 0.08	1.22 ± 0.12	0.93 ± 0.09	0.96 ± 0.1	1.06 ± 0.11
Th (ppm)	6.04 ± 0.6	4.93 ± 0.49	8.97 ± 0.9	6.85 ± 0.69	7.86 ± 0.79	9.36 ± 0.94
K (%)	0.108 ± 0.005	0.075 ± 0.004	0.033 ± 0.002	0.033 ± 0.002	0.025 ± 0.001	0.017 ± 0.001
Moisture (%)	17 ± 7	17 ± 7	17 ± 7	17 ± 7	17 ± 7	17 ± 7
Cosmic D' (Gy/ka)	0.2 ± 0.1	0.2 ± 0.05	0.2 ± 0.1	0.2 ± 0.05	0.19 ± 0.03	0.18 ± 0.02
Total D' (Gy/ka)	0.84 ± 0.12	0.68 ± 0.07	0.96 ± 0.13	0.78 ± 0.08	0.83 ± 0.08	0.92 ± 0.09
Age (years)	59 ± 15	1408 ± 196	124 ± 136	523 ± 138	2660 ± 270	4370 ± 470
Sample ID	**CON09-8-4**	**CON09-8-25**	**CON09-8-48**	**CON09-8-81**	**CON09-8-105**	
D_e (Gy)	0.9 ± 0.1	2.05 ± 0.09	9.01 ± 0.33	14.53 ± 0.22	25 ± 0.4	
n	29	19	38	40	30	
Depth (m)	0.04 ± 0.01	0.25 ± 0.05	0.48 ± 0.05	0.81 ± 0.05	1.05 ± 0.05	
Min. grain size (mm)	150-210	150-210	150-210	150-210	150-210	
U (ppm)	1.18 ± 0.12	1.84 ± 0.18	1.24 ± 0.12	1.2 ± 0.12	1.38 ± 0.14	
Th (ppm)	6.92 ± 0.69	9.24 ± 0.92	8.86 ± 0.89	10.45 ± 1.05	11.13 ± 1.11	
K (%)	0.007 ± 0	0.001 ± 0	0.013 ± 0.001	0.008 ± 0	0 ± 0	

Moisture (%)	17 ± 7	17 ± 7	17 ± 7	17 ± 7	17 ± 7	
Cosmic D' (Gy/ka)	0.2 ± 0.05	0.2 ± 0.04	0.19 ± 0.02	0.18 ± 0.02	0.18 ± 0.02	
Total D' (Gy/ka)	0.82 ± 0.09	1.07 ± 0.11	0.93 ± 0.09	1 ± 0.1	1.06 ± 0.1	
Age (years)	1096 ± 168	1921 ± 208	9650 ± 972	14490 ± 1407	23513 ± 2312	
Sample ID	**CON09-10-3**	**CON09-10-50**	**CON09-10-70**	**CON09-10-86**	**CON09-10-96**	**CON09-10-106**
D_e (Gy)	0.13 ± 0.08	1.77 ± 0.05	3.57 ± 0.27	3.07 ± 0.14	2.86 ± 0.14	5.69 ± 0.13
n	82	77	82	75	36	59
Depth (m)	0.03 ± 0.01	0.5 ± 0.05	0.7 ± 0.05	0.86 ± 0.05	0.96 ± 0.05	1.06 ± 0.05
Min. grain size (mm)	150-210	150-210	150-210	150-210	150-210	150-210
U (ppm)	0.58 ± 0.06	0.97 ± 0.1	0.99 ± 0.1	1 ± 0.1	0.89 ± 0.09	1.04 ± 0.1
Th (ppm)	6.73 ± 0.67	13.72 ± 1.37	14.37 ± 1.44	13.12 ± 1.31	12.86 ± 1.29	15.31 ± 1.53
K (%)	0.025 ± 0.001	0.041 ± 0.002	0.041 ± 0.002	0.041 ± 0.002	0.033 ± 0.002	0.041 ± 0.002
Moisture (%)	17 ± 7	17 ± 7	17 ± 7	17 ± 7	17 ± 7	17 ± 7
Cosmic D' (Gy/ka)	0.2 ± 0.07	0.19 ± 0.02	0.18 ± 0.02	0.18 ± 0.02	0.18 ± 0.02	0.18 ± 0.01
Total D' (Gy/ka)	0.71 ± 0.09	1.18 ± 0.12	1.21 ± 0.12	1.14 ± 0.11	1.09 ± 0.11	1.26 ± 0.13
Age (years)	183 ± 115	1503 ± 158	2945 ± 373	2694 ± 296	2613 ± 292	4498 ± 474
Sample ID	**CON09-13-2**	**CON09-13-20**	**CON09-13-40**	**CON09-13-55**	**CON09-13-65**	**CON09-14-17**
D_e (Gy)	0.06 ± 0.02	0.2 ± 0.04	1.14 ± 0.44	2.27 ± 0.67	3.01 ± 2.25	0.25 ± 0.08
n	42	78	25	49	11	35
Depth (m)	0.02 ± 0.01	0.2 ± 0.05	0.4 ± 0.05	0.55 ± 0.05	0.65 ± 0.05	0.17 ± 0.05
Min. grain size (mm)	150-210	150-210	150-210	150-210	150-210	150-210
U (ppm)	0.89 ± 0.09	0.95 ± 0.09	1.01 ± 0.1	0.91 ± 0.09	1.02 ± 0.1	0.79 ± 0.08
Th (ppm)	10.45 ± 1.05	10.82 ± 1.08	15.96 ± 1.6	14.57 ± 1.46	16.44 ± 1.64	2.45 ± 0.25
K (%)	0.058 ± 0.003	0.066 ± 0.003	0.066 ± 0.003	0.058 ± 0.003	0.066 ± 0.003	0 ± 0
Moisture (%)	17 ± 7	17 ± 7	17 ± 7	17 ± 7	17 ± 7	17 ± 7
Cosmic D' (Gy/ka)	0.2 ± 0.1	0.2 ± 0.05	0.19 ± 0.03	0.19 ± 0.02	0.19 ± 0.02	0.2 ± 0.06
Total D' (Gy/ka)	1 ± 0.14	1.04 ± 0.11	1.33 ± 0.14	1.22 ± 0.12	1.35 ± 0.14	0.49 ± 0.07
Age (years)	57 ± 20	189 ± 40	856 ± 344	1854 ± 578	2226 ± 1681	513 ± 179
Sample ID	**CON09-14-41**	**CON09-14-77**	**CON09-16-4**	**CON09-16-79**	**CON09-16-119**	**CON09-16-159**
D_e (Gy)	0.55 ± 0.02	0.73 ± 0.04	0.24 ± 0.01	4.42 ± 0.14	14.59 ± 0.07	17.51 ± 0.17
n	74	43	75	75	75	37
Depth (m)	0.41 ± 0.05	0.77 ± 0.05	0.04 ± 0.01	0.79 ± 0.5	1.19 ± 0.5	1.59 ± 0.5
Min. grain size (mm)	150-210	150-210	150-210	150-210	150-210	150-210
U (ppm)	0.62 ± 0.06	0.7 ± 0.07	0.68 ± 0.07	0.64 ± 0.06	0.9 ± 0.09	0.84 ± 0.08
Th (ppm)	2.2 ± 0.22	2.76 ± 0.28	3.76 ± 0.38	5.19 ± 0.52	7.51 ± 0.75	9.98 ± 1

Appendix 3. Age-depth models for each core run in CLAM. Light blue represent OSL dates except for Core15 where they are ^{210}Pb dates. Blue represents ^{14}C-AMS dates.

Appendix 4. Plots showing a non-linear temporal trend in charcoal influx per forest type. Bins in cal yr BP. Y axis was truncated at 0.5 rather than 3 (the maximum value) to observe trends.

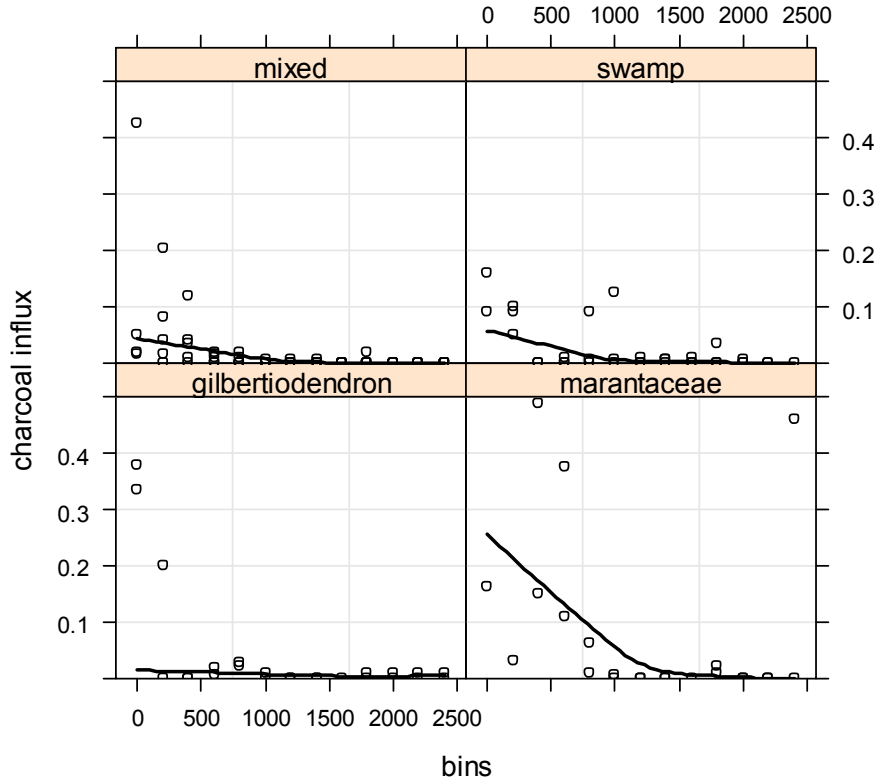

Appendix 5. Details of the additive models tested to relate charcoal influx to forest type and time (bin).

Model	Variance structure	Correlation structure	AIC	R-squared
Baseline	-	-	62.20	0.207
A	Different standard deviations per core. Formula: ~1 | core		-429.53	0.680
B	Different standard deviations per forest type. Formula: ~1 | forest_name		-316.57	0.408
C	Different standard deviations per forest type. Formula: ~1 | forest_name	Compound symmetry. Formula: ~bin	-314.75	0.410
D	Different standard deviations per forest type. Formula: ~1 | core	corAR1 Formula: ~bin	-427.53	0.680
E	Different standard deviations per forest type. Formula: ~1 | core	corAR1 Formula: ~ bin|core	-427.53	0.680

Appendix 6. Cluster analysis to identify periods (time-zones) where charcoal patterns are different. Method used: CONSLINK (constrained single-link analysis).

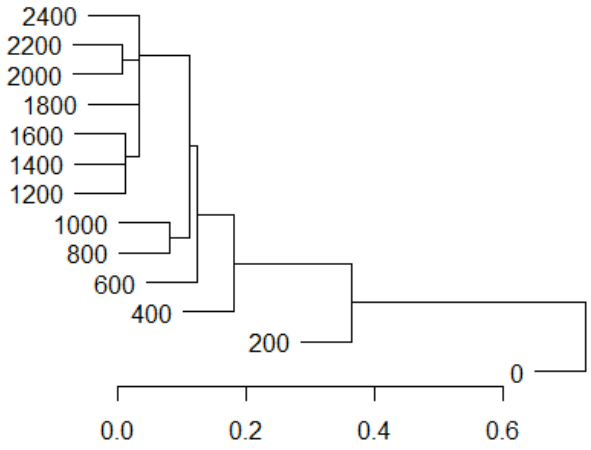

Appendix 7 Charcoal influx values for each core for the last 2,500 cal. yr BP (particles/cm^2/yr). The four different periods identified by using the zonation procedure with the 200-yr bin data (see Appendix 6) shown in Fig. 2 were overlayed: I) Minimal fires (2,500-1,100 cal yr BP), II) First occurrences of fires (1,100-500 cal yr BP), III) Increasing fires (500-300 cal yr BP), IV) Highest peaks of charcoal (300-0 cal yr BP). Site 13 is shown at a different scale.

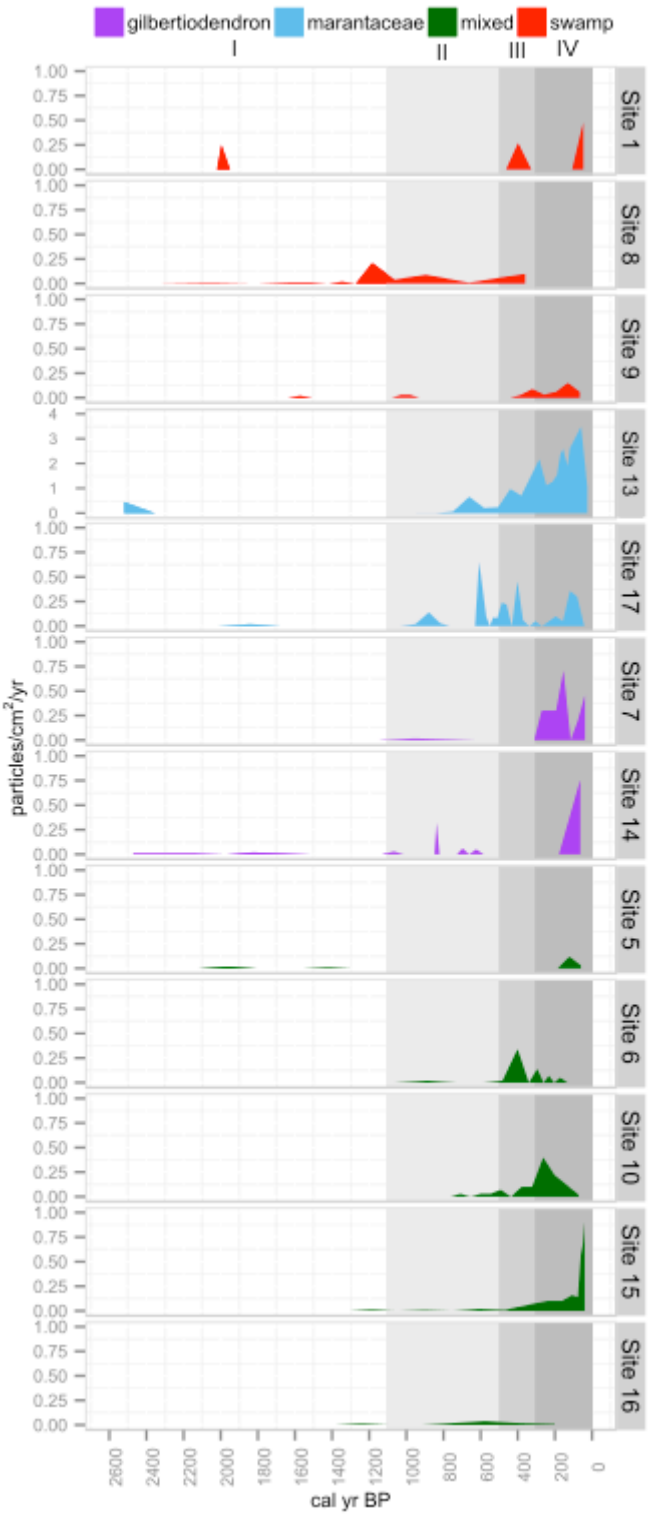

Appendix 8. Spatial autocorrelation test (Moran's I) to assess if charcoal values were clustered, overdispersed or randomly distributed over space for each bin of 200 yr.

Bin (range of cal yr BP)	Morans I	Z-scores (standard deviations)	p-value	Observations
0 – 200	-0.078	0.2339	>0.1	Random
200 – 400	-0.0403	0.5051	>0.1	Random
400 – 600	-0.1275	-0.0993	>0.1	Random
600 – 800	-0.0412	0.7147	>0.1	Random
800 – 1000	-0.3652	-1.4018	>0.1	Random
1000 – 1200	-0.144	-0.4986	>0.1	Random
1200 – 1400	-0.1881	-0.3950	>0.1	Random
1400 – 1600	-0.2165	-0.3753	>0.1	Random
1600 – 1800	-0.1924	-1.2124	>0.1	Random
1800 – 2000	-0.3364	-0.8974	>0.1	Random
2000 – 2200	-0.3556	-0.9976	>0.1	Random
2200 – 2400	-0.25	-1.1410	>0.1	Random
2400 – 2600	-0.0753	0.5472	>0.1	Random

Appendix 9. Boxplots showing fire frequency per forest type based on number of 200-year bins with presence of charcoal. Different thresholds were used to define presence or absence of fire (30th, 40th, 50th, 60th, 70th percentiles of charcoal influx values) as a sensitivity analysis.

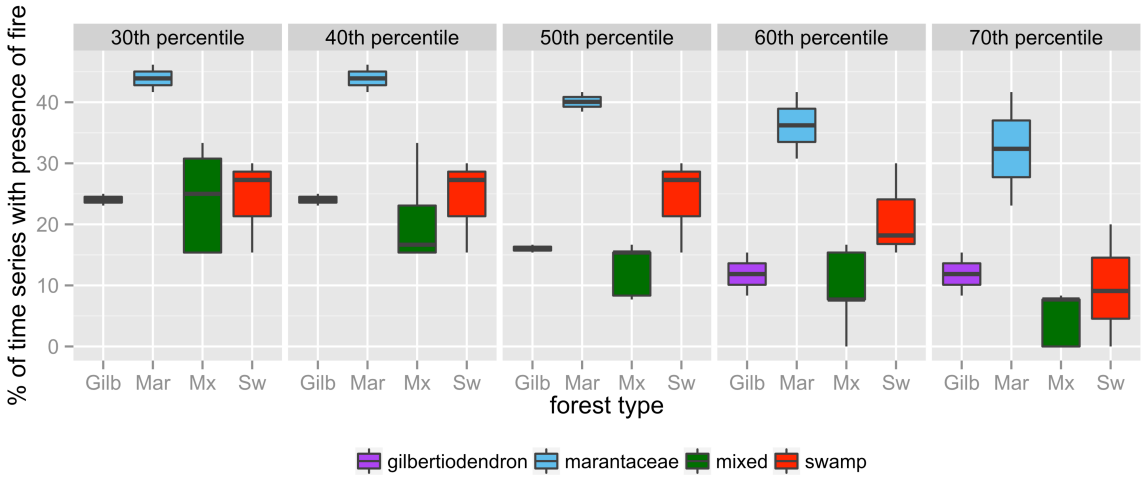

Appendix 10. Estimated smoother for the GAMM (solid line) and the 95% point-wise confidence bands (dotted line). The horizontal axis represents the 200-year bin in cal. yr BP and the vertical axis the contribution of the smother to the fitted values.